Desalination and Water Treatment
www.deswater.com

doi: 10.5004/dwt.2020.26152

202 (2020) 420–434
October

Removal of crystal violet in aqueous solution by activated carbon from the pericarp of rubber fruit and bagasse: kinetics, thermodynamics and adsorption studies

Fareeda Hayeeye[a,*], Memoon Sattar[b]

[a]*Department of Science, Faculty of Science and Technology, Prince of Songkla University, Pattani Campus, Thailand, Tel. 08-8784-1147; email: fareeda.ha@psu.ac.th (F. Hayeeye)*
[b]*Department of Science and Technology, Faculty of Sports and Health Science, Thailand National Sports University, Yala Campus, Thailand*

Received 3 May 2019; Accepted 23 May 2020

ABSTRACT

Activated carbons prepared from the pericarp of rubber fruit (PrAC) or from bagasse (BAC) were compared with a commercial activated carbon (CAC) in an adsorption and desorption study of crystal violet in aqueous solution. The adsorbents were characterized by scanning electron microscopy, as well as for specific surface and pore size distribution from Brunauer–Emmett–Teller, Fourier-transform infrared spectroscopy, and the point of zero charge (pH_{pzc}). The effects of adsorbent dosage, contact time, initial concentration of crystal violet, pH, and temperature were studied. The Langmuir adsorption isotherm fit well, and the calculated maximum adsorption capacities (q_m) were 896.7, 432.66, and 351.12 mg g^{-1} at 60°C and pH 5.0 for CAC, PrAC, and BAC, respectively. The desorption study confirmed that PrAC, BAC, and CAC can be regenerated. The adsorption of crystal violet by PrAC, BAC, or CAC was endothermic and spontaneous. The heats of adsorption ($\Delta H°$/kJ mol^{-1} = 18.43 for PrAC, 16.49 for BAC, and 30.82 for CAC) confirmed physisorption as adsorption mechanism. The maximum desorption percentages of crystal violet solution were 67.08, 46.32, and 40.64 for CAC, PrAC, and BAC at pH 2.03, indicating that PrAC and BAC can be reused in an economic treatment process.

Keywords: Activated carbon; Pericarp of rubber fruit; Bagasse; Crystal violet; Adsorption

1. Introduction

Dyes cause a lot of pollution in the environment. The water used to clean equipment and plant areas becomes wastewater and can carry foul-smelling or toxic substances into rivers. It is estimated that textile industries release weekly approximately 100 tons of dyes and pigments into the rivers [1,2]. Degradable organic dyes reduce the amount of dissolved oxygen in water, which affects living organisms and obstructs the light necessary for photosynthesis.

Crystal violet, or gentian violet, is a basic dye that is used in many applications as a pH indicator (yellow to violet transition at pH 1.6). In the medical community, it is the active ingredient in gram stain used to classify bacteria, a dermatological agent, a veterinary medicine; and it is used in industries such as textile dyeing and paper printing. The triphenylmethane groups in its structure are potentially carcinogenic, and crystal violet will destroy cells. Therefore it can be used as a disinfectant. The ability of crystal violet to bind to DNA is useful in cell viability assays, but also causes replication errors in living tissue, possibly leading to

* Corresponding author.

mutations and cancer [3]. So, to protect the ecosystem and human health, wastewater containing crystal violet must be purified by an effective method before release to the natural environment.

The removal of color from dye-bearing effluents is a major problem because of the difficulty in treating such wastewater by conventional treatment methods. There are various methods of treatment: ultrafiltration [4], coagulation [5], ion exchange [6], photocatalysis [7], and adsorption [8–10], the last of which is a particularly interesting method. Adsorption is cost-effective in the removal of dyes from wastewater, and the adsorbents used include chitosan [11], zeolite [12], and activated carbon [13–16]. Adsorption to activated carbon utilizes its large specific surface, microporous structure, high adsorption capacity, and high surface reactivity [17], but commercial activated carbon (CAC) is expensive. Many agricultural wastes have been converted into effective low-cost adsorbents. The total cost for the preparation of 1 kg of adsorbent was reported as 15.71, 39.45, 2.21, and 15.13 THB (Thai Baht) for activated tamarind seeds, activated leaves, sawdust, and activated fly ash, respectively [18]. Agricultural wastes have been tested for the removal of crystal violet, namely rice husk [19], potato peels [20], male flowers of the coconut tree [21], and bamboo leaves [22], but the adsorption capacities were low. There are several studies on adsorption by activated carbon, not on using pericarp of rubber fruit or bagasse converted to active carbon. Thus, this study prepared activated carbon from the pericarp of rubber fruit (PrAC) and bagasse (BAC), utilizing agricultural wastes easily accessible in Thailand, and compared these with CAC for their potential to remove crystal violet from aqueous solution, in order to replace expensive CAC in the treatment of wastewater.

2. Materials and methods

2.1. Materials

The CAC was obtained from Sigma-Aldrich, UK. The pericarp of rubber fruit and bagasse agricultural wastes were collected from Hat Yai, Thailand. Zinc chloride, $ZnCl_2$ A.R., 98%, was purchased from Sigma-Aldrich. Crystal violet came from BDH Chemicals Ltd., Poole, UK. Sodium hydroxide, NaOH A.R., 99%, and hydrochloric acid, HCl A.R., 37%, used for pH adjustment, were purchased from Labscan Ireland and Merck, Germany, respectively.

2.2. Preparation of PrAC and BAC adsorbents

The activated carbons from the pericarp of rubber fruit (PrAC) and bagasse (BAC) were produced by carbonization and chemical activation with $ZnCl_2$. The activated carbon produced by $ZnCl_2$ activation is dominantly microporous, but with a significant component of mesopores that increases with the impregnation ratio ($ZnCl_2$/precursor) [23,24]. For carbonization, the pericarp of rubber fruit and bagasse were dried and cut to small approximately 1-inch square pieces, which were carbonized in a muffle furnace at 400°C for 1 h under atmospheric conditions. This caused thermal decomposition, phase transitions, and removal of volatile components. After carbonization, the residual char was ground and graded by sieve sizing to 140–170 mesh fraction. The ground char was chemically activated by mixing with a concentrated solution of $ZnCl_2$ at a ratio of 1:2. The mixture was heated at 600°C for 3 h in the muffle furnace and, when removed from the furnace, the activated carbon was washed with a 1% HCl solution. It was then soaked in hot water for 5 min and the water was drained through a Buchner funnel. This washing step was repeated two more times to obtain a neutral pH. Finally, the activated carbon (AC) was dried in an oven at 110°C for 24 h. The PrAC and BAC were kept in desiccators [25]. The oven-dried PrAC and BAC were powdered and sieved to 140–170 mesh fractions [26] and stored in desiccators until use in crystal violet sorption experiments.

2.3. PrAC, BAC and CAC adsorbent characterizations

A scanning electron microscopy (SEM) (JSM-5800 LV at Scientific Equipment Center of PSU, Thailand) was used to analyze the morphology and porosity of the PrAC, BAC, and CAC adsorbents.

Brunauer–Emmett–Teller (BET) specific surface areas of PrAC, BAC, and CAC were determined from nitrogen adsorption isotherms at 77 K produced with a Coulter SA 3100 analyzer (Thailand). The pore size distribution was calculated from the Barrett–Joyner–Halenda (BJH) model. (The measurements were conducted at the Department of Chemical Engineering, PSU, Thailand).

The Fourier-transform infrared spectroscopy (FT-IR) spectra of PrAC and BAC were recorded with an FT-IR spectrophotometer (Spectrum GX, Perkin Elmer, U.S.) over the wavelength range from 4,000 to 400 cm^{-1}. The transmission infrared spectra of the carbon samples were obtained using the KBr technique. The KBr pellets were prepared from activated carbon-KBr mixtures at a ratio of approximately 1:300. Before the spectrum of a sample was recorded, a background line was obtained arbitrarily and subtracted. The spectra were recorded at a scan rate of 0.2 cm s^{-1}, and for better resolution, the data of the interferogram at a resolution of 4 cm^{-1} were scanned more than 10 times.

The point of zero charge (pH_{pzc}), at which the surface of an adsorbent is neutral, was determined for PrAC, BAC, and CAC by the pH drift method [27]. The pH of 0.1 M NaCl solution was adjusted to a value from 2 to 12, and the adsorbent was added into 100 mL of the pH-adjusted NaCl. The flasks were sealed to eliminate any contact with air and left at ambient temperature. The final pH was recorded after it had stabilized (typically after 24 h). The pH_{pzc} value of activated carbon was the point at which the initial pH and the final pH_f were equal, obtained from the graph of final pH_f vs. initial pH_0.

2.4. Adsorbate (crystal violet) solution

Crystal violet ($C_{25}H_{30}N_3Cl$, MW 407.98 g mol^{-1}, solubility in water 16 g L^{-1}at 25°C) is the adsorbate in this study. A stock solution was prepared by dissolving an accurately weighed quantity of crystal violet to have 1,000 mg L^{-1} distilled water concentration. The experimental solutions at the desired concentrations were prepared by diluting the stock solution with distilled water, to obtain a series of

standard solutions with concentrations ranging from 250 to 500 mg L^{-1}. The concentration of the crystal violet solution was measured by UV-Visible spectrophotometry at 591 nm.

2.5. Adsorption experiments

In the adsorption tests, 0.03 g of PrAC, 0.05 g of BAC or 0.02 g of CAC was added into 50 mL of crystal violet solution Adsorption equilibrium studies of crystal violet on PrAC, BAC and CAC were carried out by a batch equilibration method at 30°C, 40°C, 50°C, and 60°C. The concentrations of crystal violet in solutions at pH 5.0 (natural pH of solution) varied in the range from 250 to 500 mg L^{-1}. After gentle shaking to reach equilibrium, the contents were centrifuged. UV-Vis spectrophotometry at 591 nm determined concentrations of crystal violet before and after adsorption. The adsorption capacity, q_e (mmol g^{-1}), and the percentages of crystal violet adsorbed were calculated from Eqs. (1) and (2), respectively [28]:

$$q_e = \frac{V\left(C_0 - C_e\right)}{W} \tag{1}$$

$$\%\text{adsorbed} = \frac{C_0 - C_e}{C_e} \times 100 \tag{2}$$

where q_e is the adsorption capacity (mmol g^{-1}), V is the volume of the solution (L), C_0 is the initial concentration of crystal violet (mmol L^{-1}), C_e is the equilibrium concentration of crystal violet (mmol L^{-1}) and W is the mass of the adsorbent (g).

The effects of adsorbent dosage, contact time, pH and temperature were also studied. All of the adsorption experiments used 50 mL of 300 mg L^{-1} crystal violet solution at pH 5, which is the natural pH of crystal violet aqueous solution. All experiments were conducted in triplicates. To determine the effects of pH, the initial pH of the dye solution was adjusted to between 2 and 10 using HCl or NaOH solutions. The equilibrium data were used in studies of kinetic adsorption, adsorption isotherms, and thermodynamics.

Kinetic experiments were conducted on crystal violet solutions at initial concentrations of 300, 400, and 500 mg L^{-1} and at a constant initial pH of 5.0. PrAC (0.03 g), BAC (0.05 g) or CAC (0.02 g) was added into 50 mL of crystal violet solution, which was then continuously shaken. Solution samples of 1 ml were withdrawn with a syringe at pre-determined sampling times and analyzed for residual crystal violet by UV-Vis spectrophotometry at 591 nm.

2.6. Equation models for adsorption kinetics, isotherms and thermodynamic studies

2.6.1. Kinetic adsorption models

The pseudo-first-order model can be expressed by the Lagergren equation [29] and the pseudo-second-order model by the expression reported by Ho and McKay [30]. They are shown in Eqs. (3) and (5), respectively, and integrating these into linear form gives Eqs. (4) and (6):

$$\frac{dq_t}{dt} = k_1\left(q_e - q_t\right) \tag{3}$$

$$\ln\left(q_e - q_t\right) = \ln q_e - k_1 t \tag{4}$$

$$\frac{dq_t}{dt} = k_2\left(q_e - q_t\right)^2 \tag{5}$$

$$\frac{t}{q_t} = \frac{1}{k_2 q_e^2} + \frac{1}{q_e} t \tag{6}$$

where q_e and q_t are the amounts of dye adsorbed (mmol g^{-1}) at equilibrium and at any time t, k_1 is the rate constant (min^{-1}), and k_2 is the second-order rate constant (g $mmol^{-1}$ min^{-1}).

The adsorption process can be separated into three stages: external surface adsorption, gradual adsorption when intraparticle diffusion is rate-controlling, and interior surface adsorption that is the final equilibration stage [31].

The intraparticle diffusion model proposed by Weber and Morris [32] is shown in Eq. (7):

$$q_t = k_p t^{1/2} + C \tag{7}$$

where k_p is the intraparticle diffusion rate constant (mg g^{-1} $min^{-1/2}$).

The nature of initial adsorption behavior can be explained by the initial factor based on the intraparticle diffusion model. In the first instance, Eq. (7) can be written as:

$$q_{\text{ref}} = k_p t_{\text{ref}}^{1/2} + C \tag{8}$$

where t_{ref} is the longest time of adsorption and q_{ref} is the amount adsorbed at t_{ref}. The difference of Eqs. (8) and (7) gives:

$$q_{\text{ref}} - q_t = k_p\left(t_{\text{ref}}^{1/2} - t^{1/2}\right) \tag{9}$$

Rearrangement of Eq. (9) yields:

$$\left(\frac{q_t}{q_{\text{ref}}}\right) = 1 - R_i\left[1 - \left(\frac{t}{t_{\text{ref}}}\right)^{1/2}\right] \tag{10}$$

where R_i is defined as the initial factor based on the intraparticle diffusion model and is expressed in Eq. (11):

$$R_i = \frac{q_{\text{ref}} - C}{q_{\text{ref}}} \tag{11}$$

Values of R_i are categorized into four zones: $0.9 < R_i < 1.0$ indicates weak initial adsorption (zone 1); $0.5 < R_i < 0.9$ for intermediate initial adsorption (zone 2); $0.1 < R_i < 0.5$, for strong initial adsorption (zone 3); and $R_i < 0.1$ for approaching complete initial adsorption (zone 4) [33].

2.6.2. Adsorption isotherm models

The Langmuir isotherm [34] is still the most common model of adsorption. The non-linear form of Langmuir

isotherm is shown in Eqs. (12) and (13). The Freundlich isotherm [35] is an empirical equation employed to describe heterogeneous systems, expressed by Eqs. (14) and (15).

$$q_e = \frac{q_m b C_e}{1 + b C_e} \tag{12}$$

$$\frac{C_e}{q_e} = \frac{1}{q_m b} + \frac{C_e}{q_m} \tag{13}$$

$$q_e = K_F C_e^{1/n} \tag{14}$$

$$\ln q_e = \ln K_F + \frac{1}{n} \ln C_e \tag{15}$$

where C_e is the equilibrium concentration of crystal violet (mmol L^{-1}), q_e is the amount adsorbed at equilibrium (mmol g^{-1}) and q_m and b are Langmuir constants. In fact, q_m is related to the maximum adsorption capacity (mmol g^{-1}) and b is the adsorption equilibrium constant (L $mmol^{-1}$). K_F (L g^{-1}) is the so-called unit capacity factor that shows adsorption capacity, and n is an empirical parameter representing the heterogeneity of the site energies and also is indicative of the intensity of adsorption. Cases with $n > 1$ are favorable to adsorption [36].

2.6.3. Thermodynamic studies

The temperature dependence of crystal violet adsorption on PrAC, BAC or CAC was assessed from assays at the four temperatures 30°C, 40°C, 50°C and 60°C. The thermodynamic parameters were calculated from the van't Hoff Eq. (16) [37]:

$$\ln K_c = \frac{\Delta S^\circ}{R} - \frac{\Delta H^\circ}{RT} \tag{16}$$

Enthalpy (ΔH°) and entropy (ΔS°) were estimated from the slope and intercept and the Gibbs free energy (ΔG°) was determined from Eq. (17):

$$\Delta G^\circ = \Delta H^\circ - T\Delta S^\circ \tag{17}$$

where K_c is the ratio of C_A (the solid-phase concentration of crystal violet at equilibrium in mmol L^{-1}) to C_e (the equilibrium concentration of crystal violet in solution in mmol L^{-1}), R is the universal gas constant (8.314 J K^{-1} mol^{-1}), and T is the absolute temperature (K).

2.7. Desorption studies

Crystal violet in aqueous solution (300 mg L^{-1}) was adsorbed on PrAC, BAC, or CAC adsorbent until equilibrium was achieved. The PrAC, BAC, or CAC was centrifuged out of the suspension and dried at 110°C. Aqueous solutions were prepared for desorption studies by adjusting distilled water to various pH 2–9 with either 0.1 M NaOH or HCl. PrAC, BAC, or CAC was added into 50 mL of each of these solutions and agitated at 30°C for 24 h. To determine the concentration of crystal violet in solution after desorption, absorbance at 591 nm was determined by UV-Vis spectrophotometry (UV 2600, Shimadzu, Thailand) and the percentage desorption of crystal violet to the solution was then calculated from Eq. (18) [38]:

$$\%\text{desorption} = \frac{M_{\text{de}}}{M_{\text{ad}}} \times 100 \tag{18}$$

where M_{de} and M_{ad} are the mass of crystal violet desorbed and adsorbed, respectively.

3. Results and discussion

3.1. Characterization of PrAC and BAC

3.1.1. Scanning electron microscopy

The SEM micrographs of the morphology of the adsorbents PrAC and BAC in powder form (140–170 mesh) (Fig. 1) shows the porosity of PrAC and BAC caused by $ZnCl_2$ activation. The PrAC and BAC contain numerous pores with diameters ranging from around 9.5 to 19.5 μm and from 5 to 10 μm, respectively. The pores in PrAC, BAC, and CAC were classified as macropores (>50 nm). Micropores and mesopores could not be resolved by SEM even at a higher magnification, possibly because of the limit of detection of the instrument.

3.1.2. Specific surface area

The specific surface and pore size distribution of PrAC, BAC, and CAC were estimated from the BET [39] and the BJH models [40], respectively. The N_2 adsorption isotherms (Fig. 2) can be classified into two types. According to the International Union of Pure and Applied Chemistry classification, the isotherm of the BAC sample approximately types I, but the isotherm for PrAC is of mixed type. Unlike other activated carbons, the present samples did not reach a clear plateau. This indicates that PrAC and BAC are mainly micro- and mesoporous in character, with a minor presence of larger pores, where capillary condensation occurred [41]. The calculated BET surface areas of PrAC and BAC (Table 1) differ. The BET surface area of CAC is the highest. The adsorption efficiency may be affected by the BET specific surface area. Micropores are widely evaluated by using the potential theory of Dubin, and *t*-plot, *α*-plot, or MP methods [42]. This study used the *t*-plot method to determine the micropore surface area, micropore fraction, and micropore volume, but this method cannot be used to determine the size distribution of micropores. Pore size distribution above 2 nm, however, can be assessed accurately from the BJH model (Fig. 3) [43].

CAC possessed the largest micropore surface area and micropore volume, and the micropore areal fraction ((micropore surface area/BET surface area) × 100) was around 76%, larger than those for PrAC and BAC (Table 1). Notably, CAC had the greatest BET specific surface and greater incremental volume of mesopores than PrAC or BAC (Fig. 3). The physical characteristics of the raw materials may have already determined the nature of porosity in the respective activated carbon products.

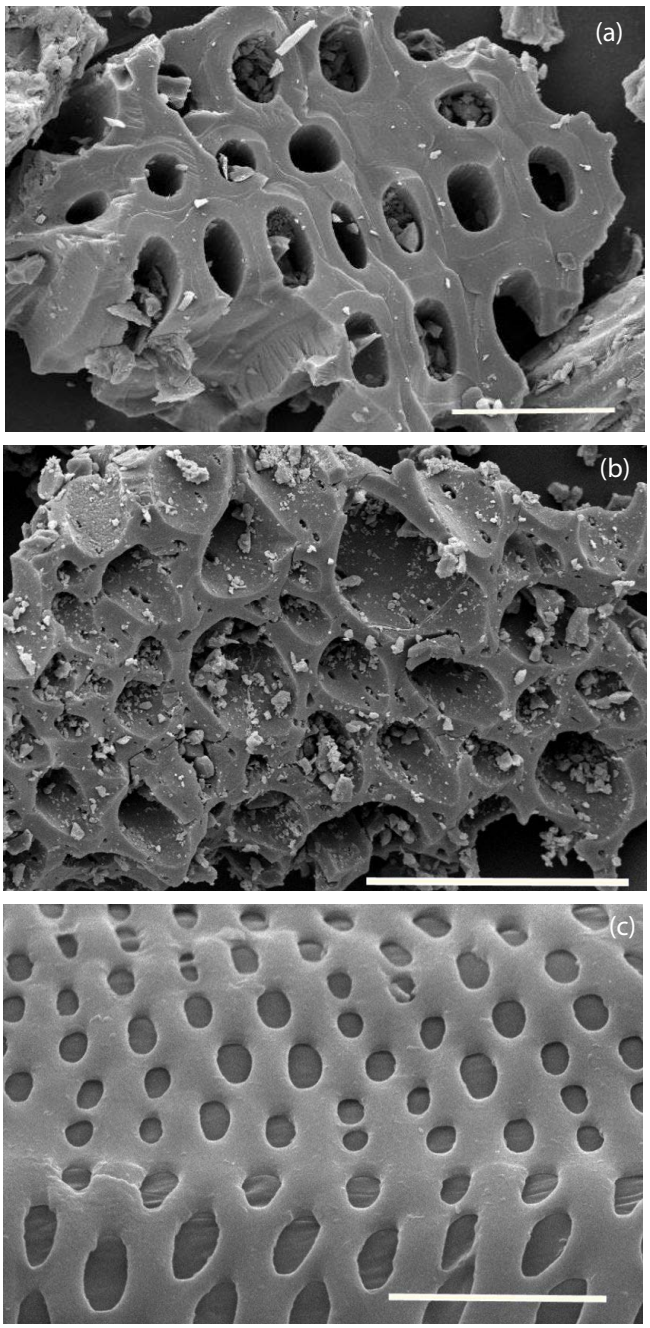

Fig. 1. SEM micrographs of (a) PrAC, (b) BAC, and (c) CAC (5,000).

BAC did not have significant volumes of mesopores or macropores (>2 nm) whereas PrAC possessed a significant volume of mesopores with the majority between 6 and 16 nm in diameter.

3.1.3. Fourier-transform infrared spectroscopy

FT-IR analysis identified the surface functional groups of PrAC and BAC. The functional groups on the surfaces of PrAC and BAC are indicated in the FT-IR spectra and the results are summarized in Table 2. The strong band at about

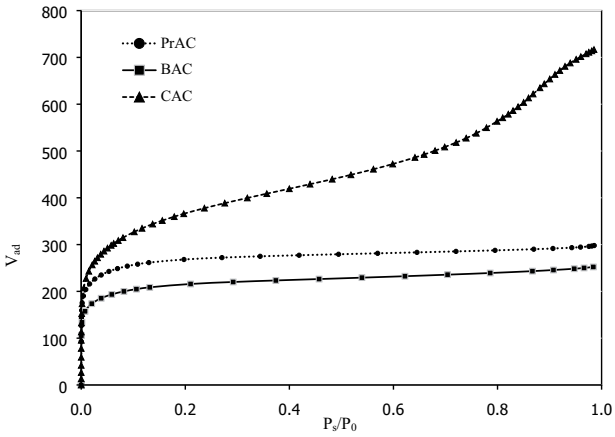

Fig. 2. N_2 adsorption isotherms for PrAC, BAC, and CAC.

3,400 cm^{-1} is mainly assigned to O–H stretching vibrations. The band observed at about 2,900 cm^{-1} is ascribed to symmetric and asymmetric C–H stretching vibrations in aliphatic CH, CH_2, and CH_3 groups. The band at about 1,600 cm^{-1} is for C=C stretching vibrations in aromatic rings. The bands observed in the range from 1,400 to 400 cm^{-1} are due to hydrogen, oxygen, and nitrogen functional groups, but it is difficult to assign each band to a specific functional group except for the strong band at about 1,020 cm^{-1}, which can be attributed to C–O stretching vibrations. The FT-IR spectra of PrAC and BAC are very similar [44].

3.1.4. Point of zero charge

The graphs of the final pH against the initial pH for the activated carbon samples were obtained by using the pH drift method. The results (Fig. 4) show that pH_{pzc} of PrAC, BAC, and CAC were 6.5, 4.5, and 3.5, respectively, so that these adsorbents were acidic in nature with negative charges. Crystal violet has a positive charge and is electrostatically attracted to these activated carbons.

3.2. Adsorption studies

3.2.1. Effects of various parameters

3.2.1.1. Weight of activated carbon

Fig. 5 shows that the percentage crystal violet adsorbed at equilibrium increased with the amount of PrAC, BAC, or CAC (0.02–0.07 g). A larger dose of PrAC, BAC, or CAC increased the availability of adsorption sites [45]. The highest adsorption capacities at equilibrium were 0.75, 0.61, and 1.52 mmol g^{-1} for PrAC, BAC, and CAC, respectively. These capacities were obtained with 0.03 g PrAC, 0.05 g BAC, and 0.02 g CAC. These doses were considered to near-optimal since the time to reach equilibrium was short, which is desirable in industrial applications [46].

3.2.1.2. Contact time and initial dye concentration

In adsorption studies, the required contact time is one aspect affecting the efficiency of an adsorbent. The rate of

Table 1
BET and micropore surface areas, with micropore fraction and volume for PrAC, BAC, and CAC

Sample	Total BET surface area ($m^2\ g^{-1}$)	Micropore surface area ($m^2\ g^{-1}$)	Micropore fraction (%)	Micropore volume ($mL\ g^{-1}$)
PrAC	920.69	698.26	75.84	0.32
BAC	786.24	573.86	72.99	0.24
CAC	1,312.34	491.65	36.48	0.18

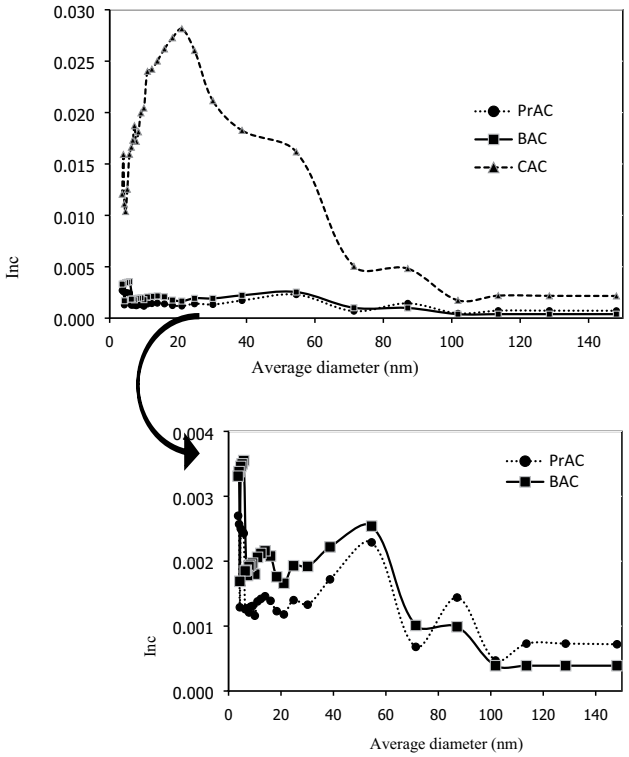

Fig. 3. BJH pore size distributions for PrAC, BAC, and CAC.

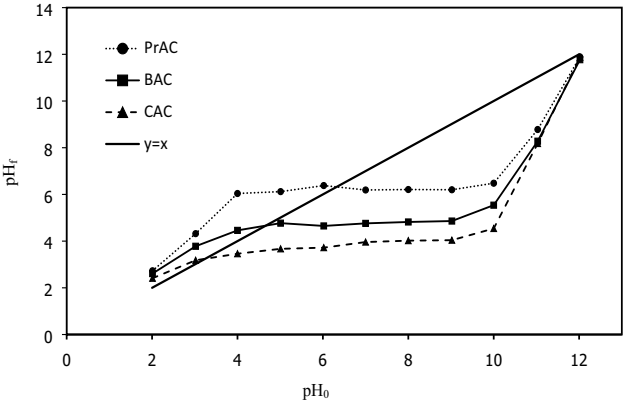

Fig. 4. The point of zero charge (pH_{pzc}) for PrAC, BAC, and CAC.

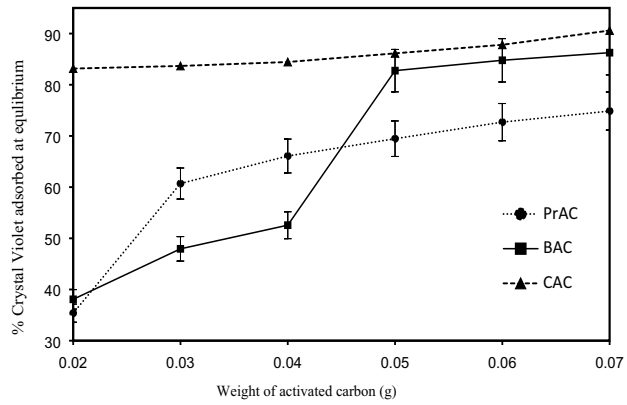

Fig. 5. Effects of dose of PrAC, BAC, and CAC (0.02–0.07 g) on adsorption of crystal violet (initially 300 mg L^{-1}) at 30°C and pH 5.0.

uptake of crystal violet was measured every 2 h on PrAC and BAC and every hour on CAC, until the equilibrium was achieved around 8, 12, and 6 h for PrAC, BAC, and CAC (Fig. 6). In the adsorption isotherm experiments, the reaction time was long enough to ensure complete equilibration.

Table 2
Surface functional groups of PrAC and BAC

Wave number (cm^{-1})	Vibrational mode	Functional group	AC type		Intensity
			PrAC	BAC	
3,400	O–H stretching	H_2O, phenol, alcohol	/	/	Strong
2,900	C–H stretching	CH_2, CH_3	/	/	Weak
1,600	C=O stretching	Carbonyl in ketone	/	/	Medium
	C=C stretching	Aromatic compound	/	/	Medium
1,400	O–H bending	Alcohol, carboxylic acid	/	/	Medium
1,050	C–O stretching	Alcohol	/	/	Strong

/ indicates that peak is detected.

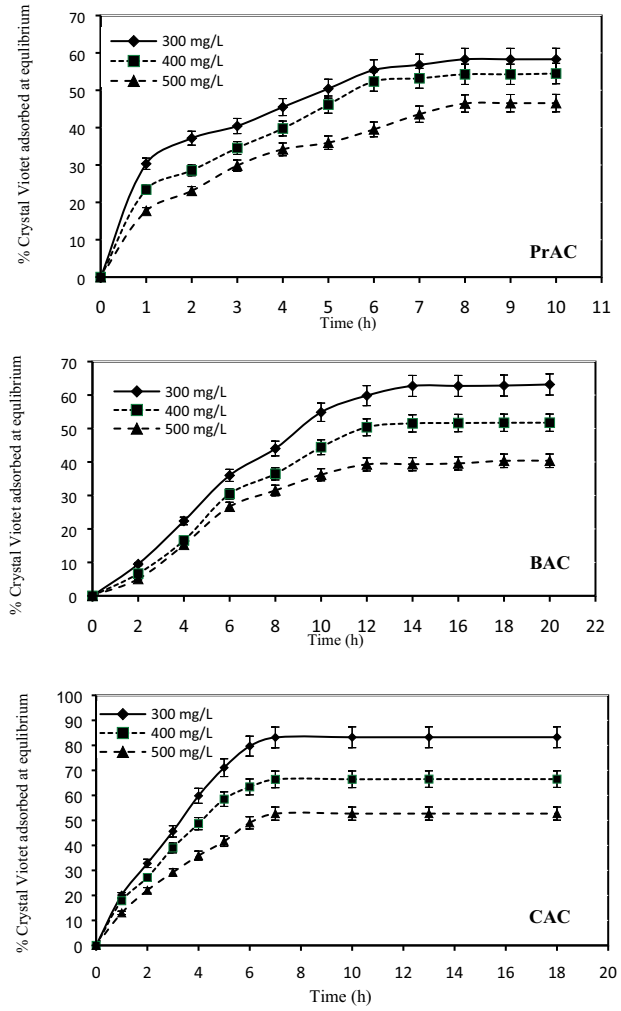

Fig. 6. Effects of contact time and initial crystal violet concentration (300, 400, or 500 mg L^{-1}) on adsorption by PrAC, BAC, and CAC, at 30°C and pH 5.0.

The results show that the amount adsorbed at equilibrium increased with the initial concentration of crystal violet (Fig. 6). It was found that the adsorption capacity, q_e, also increased with the initial concentration of crystal violet. The higher q_e was a result of the law of mass action, for a greater dye concentration [47].

3.2.1.3. pH

The general trend was a slightly increased crystal violet adsorption on activated carbon with pH (Fig. 7), above pH 2. Due to protonation at low pH, H^+ adsorption on the activated carbon surfaces competes for surface sites with the crystal violet. The surface of PrAC is positively charged at pH < pH_{pzc} (6.5) and BAC is negative for pH > pH_{pzc} (4.5). As an increasing amount of crystal violet is adsorbed, this increases the pH, so the electrical repulsion force becomes weaker and crystal violet may transfer to the surface of the activated carbon due to the action of factors such as reduced competition from protonation [48].

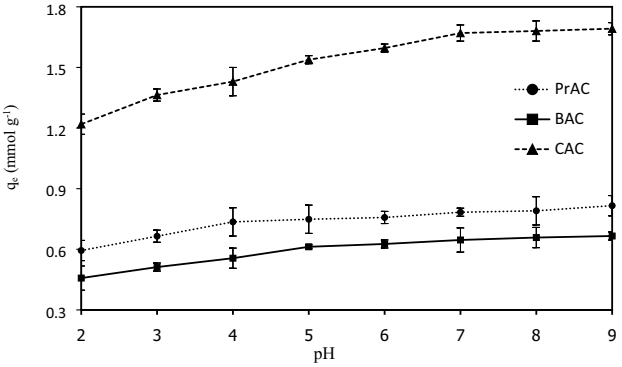

Fig. 7. Effects of pH on adsorption of crystal violet (initially 300 mg L^{-1}) by PrAC, BAC, and CAC in the pH range 2–9 at 30°C.

3.2.1.4. Temperature

The adsorption capacities of PrAC, BAC, and CAC adsorbents increased with temperatures from 30°C to 60°C (Fig. 8). This indicates that the adsorption process was endothermic [49].

3.2.2. Equilibrium models for the adsorption of crystal violet

3.2.2.1. Kinetic adsorption studies

A kinetic model predicts the effects of equilibration time on adsorption. The kinetic models (pseudo-first-order and pseudo-second-order types) and the kinetic parameters along with coefficients of determination, R^2, for the adsorption of crystal violet by PrAC, BAC, and CAC, are presented in Fig. 9 and Table 3. The values of k_1 in the pseudo-first-order model were obtained from the slopes of linear fitted lines in plots of $\ln(q_e - q_t)$ vs. t (Fig. 9a–c). The values of k_2 for the pseudo-second-order model were calculated from the slopes of the linear plots of t/q_t vs. t (Figs. 9d–f). The results show that adsorption of crystal violet on PrAC, BAC, and CAC was the best fit by the pseudo-second-order model, giving larger values of R^2 than the alternative model type tested here.

Fig. 10 and Table 4 present the intraparticle diffusion model and the rate constant k_p evaluated from the slope in the plot of q_t against $t^{1/2}$. The values of R^2 indicate that the intraparticle diffusion model gave the best fit to crystal violet sorption by PrAC, BAC, and CAC. In addition, the R_i values from the intraparticle diffusion model (which were calculated from Eq. (11)) for adsorption of crystal violet by PrAC at 50, 100, and 200 mg L^{-1} were 0.70, 0.86, and 0.91; for BAC these were 0.35, 0.57, and 0.63; and for CAC they were 0.72, 0.77, and 0.76. For crystal violet at 200 mg L^{-1} on PrAC, $0.9 < R_i < 1.0$ indicating weak initial adsorption with low external mass transfer and low initial uptake rates, known as zone 1. For crystal violet at 100 and 200 mg L^{-1} on BAC and on CAC, $0.5 < R_i < 0.9$ indicates intermediate initial adsorption or zone 2. For crystal violet at 50 mg L^{-1} on BAC, $0.1 < R_i < 0.5$ indicates strong initial adsorption, which means high initial result with high external mass transfer and high initial uptake rates, or zone 3 [33].

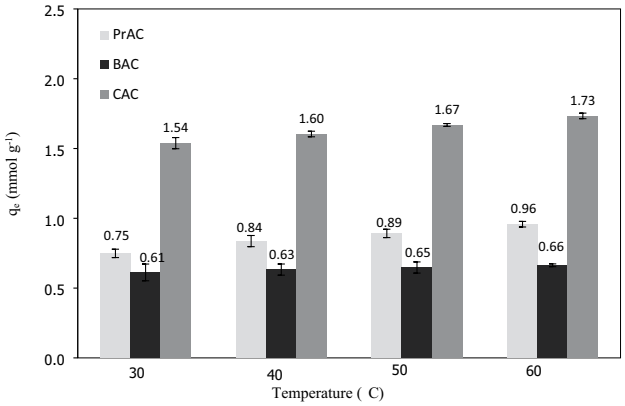

Fig. 8. Effects of temperature on adsorption of crystal violet (initially 300 mg L^{-1}) by PrAC, BAC, and CAC at 30°C, 40°C, 50°C, and 60°C, and pH 5.0.

3.2.2.2. Adsorption isotherm studies

The adsorption isotherms of crystal violet by PrAC, BAC, and CAC at various temperatures are shown in Fig. 11. The Langmuir isotherm in linear form Fig. 12a of crystal violet sorption onto PrAC, BAC and CAC were plotted: equilibrium concentrations in proportion to the adsorbed amounts of crystal violet (C_e/q_e) vs. the equilibrium concentration of crystal violet (C_e), at 30°C, 40°C, 50°C, and 60°C. The data were least-squares fit with a straight line, and R^2 for the Langmuir adsorption isotherm approached 1 at every temperature tested. The maximum adsorption capacities q_m (mmol g^{-1}) were calculated from the slope ($=1/q_m$) and the equilibrium constant related to the heat of adsorption, b (L $mmol^{-1}$), was calculated from the intercept ($=1/(bq_m)$). The values of q_m, b, and R^2 are shown in Table 5. The favorability of the adsorption was confirmed from the dimensionless separation factor (R_L). The R_L values for the adsorption of crystal violet on PrAC, BAC, and CAC were

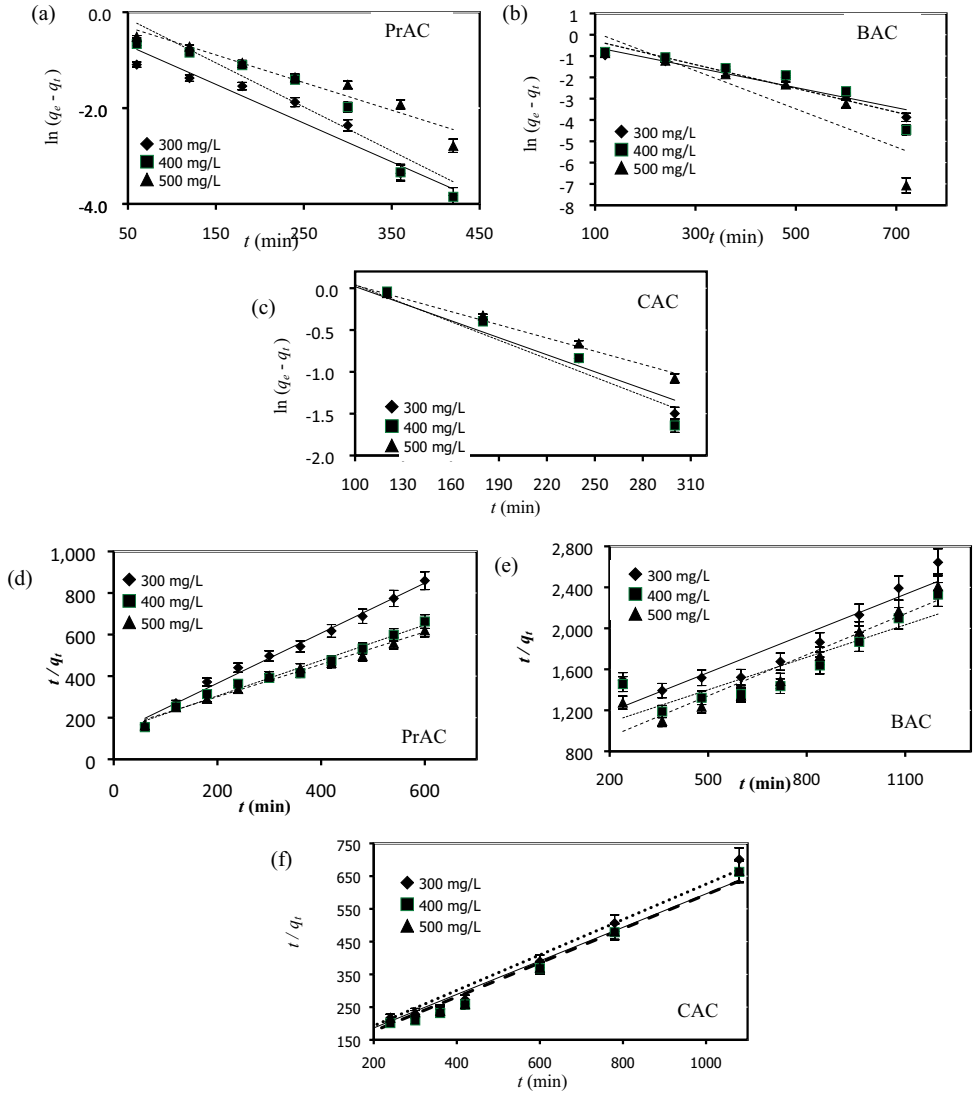

Fig. 9. Kinetic adsorption models: (a–c) pseudo-first-order and (d–f) pseudo-second-order models, for crystal violet (300, 400, and 500 mg L^{-1}) adsorption by PrAC, BAC, and CAC at 30°C and pH 5.0.

Table 3
Kinetic parameters in pseudo-first-order and pseudo-second-order models for crystal violet (300, 400, and 500 mg L^{-1}) adsorption at 30°C by PrAC, BAC, and CAC, at pH 5.0

C_0 (mg L^{-1})	$q_{e,exp.}$ (mmol g^{-1})	PrAC						$q_{e,exp.}$ (mmol g^{-1})	BAC						$q_{e,exp.}$ (mmol g^{-1})	CAC					
		Pseudo-first-order			Pseudo-second-order				Pseudo-first-order			Pseudo-second-order				Pseudo-first-order			Pseudo-second-order		
		q_e	k_1 (×10^{-3})	R^2	q_e	k_2 (×10^{-2})	R^2		q_e	k_1 (×10^{-3})	R^2	q_e	k_2 (×10^{-3})	R^2		q_e	k_1 (×10^{-3})	R^2	q_e	k_2 (×10^{-3})	R^2
300	0.69	0.75	8.1	0.92	0.83	1.16	0.99	0.45	0.89	4.7	0.94	0.75	1.28	0.90	1.54	2.01	6.8	0.97	1.75	3.4	0.99
400	0.91	1.38	9.2	0.90	1.17	5.43	0.98	0.49	1.31	5.6	0.87	0.79	1.74	0.90	1.60	2.16	7.4	0.97	1.85	2.7	0.98
500	0.97	0.97	5.8	0.93	1.28	4.21	0.99	0.51	2.72	9.0	0.78	0.95	2.64	0.91	1.62	1.64	5.3	0.97	1.82	3.7	0.96

Table 4
Intraparticle diffusion model fits for crystal violet adsorption by PrAC, BAC, and CAC at 30°C and pH 5.0

C_0 (mg L^{-1})	PrAC			BAC			CAC		
	$q_{e,exp.}$ (mmol g^{-1})	Intraparticle diffusion		$q_{e,exp.}$ (mmol g^{-1})	Intraparticle diffusion		$q_{e,exp.}$ (mmol g^{-1})	Intraparticle diffusion	
		k_p (mmol g^{-1} $min^{-1/2}$)	R^2		k_p (mmol g^{-1} $min^{-1/2}$)	R^2		k_p (mmol g^{-1} $min^{-1/2}$)	R^2
300	0.69	0.0218	0.96	0.45	0.022	0.99	1.54	0.097	0.99
400	0.91	0.0347	0.95	0.49	0.026	0.98	1.60	0.369	0.98
500	0.97	0.0384	0.98	0.51	0.024	0.96	1.62	0.383	0.96

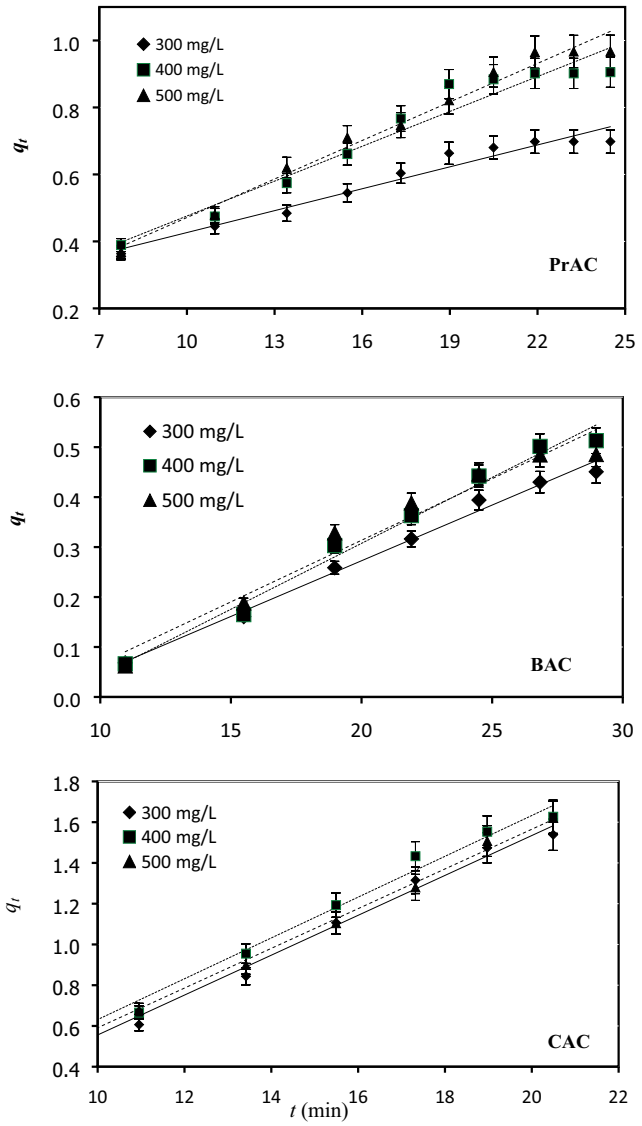

Fig. 10. Intraparticle diffusion model for the adsorption of crystal violet (300, 400, and 500 mg L^{-1}) by PrAC, BAC, and CAC at 30°C and pH 5.0.

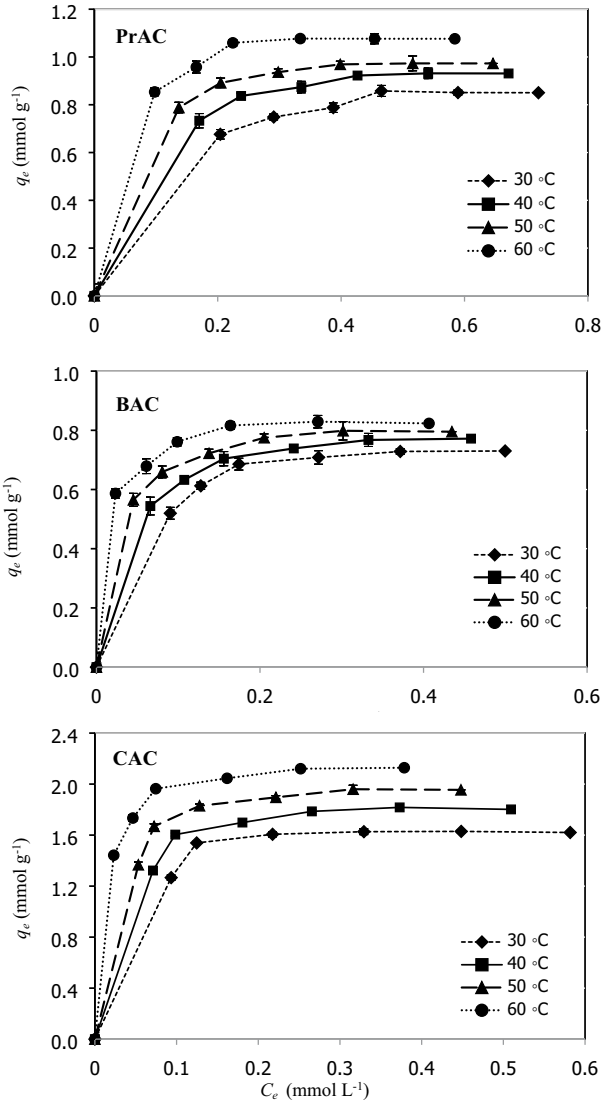

Fig. 11. Adsorption isotherms for crystal violet (250–500 mg L^{-1}) on PrAC, BAC, and CAC at 30°C, 40°C, 50°C, and 60°C and pH 5.0.

between 0 and 1, which indicates favorable adsorption [50]. To determine the parameters in the Freundlich equation (n and K_F), linear least-squares fits were applied to lnq_e against lnC_e (Fig. 12b). The K_F, n, and R^2 values are shown in Table 6. For adsorption data of crystal violet on PrAC, BAC, and CAC the coefficient of determination R^2 was better for the Langmuir than the Freundlich equation. Thus, the Langmuir equation was chosen as the best match with the adsorption isotherms.

The maximum adsorption capacities (q_m) of PrAC, BAC, and CAC for crystal violet at 60°C, estimated based on the Langmuir isotherm fits, were 896.70, 432.66, and 351.12 mg g^{-1}, respectively (Table 5). The results show that CAC and PrAC had higher maximum adsorption capacities than BAC, matching the least specific surface area of BAC. The CAC was purchased for 5,000 Thai Baht per kg, while preparing 1 kg of PrAC or BAC cost in total about 20 to 40 Baht. The maximum adsorption capacities (q_m) of PrAC and BAC were higher than the capacities reported in prior literature for similar types of adsorbents for crystal violet removal (Table 7).

3.3. Thermodynamic study

The equilibrium data showing the effects of temperature on crystal violet sorption by PrAC, BAC, and CAC were used in a thermodynamic assessment. The van't Hoff equation suggests plotting lnK_c vs. $1/T$ (Fig. 13). The graph should give a straight line segment, determined by the thermodynamic parameters enthalpy ($\Delta H°$) and entropy $\Delta S°$) that influence the slope ($-(\Delta H°/R)$) and the intercept ($\Delta S°/R$). Eq. (17) was used to calculate the Gibbs free energy ($\Delta G°$). The thermodynamic parameter estimates in

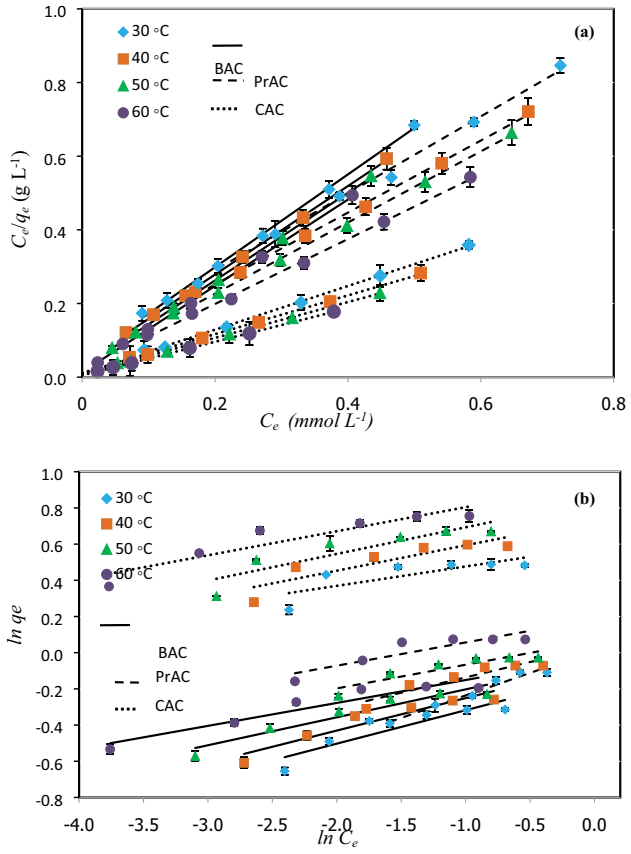

Fig. 12. (a) Langmuir and (b) Freundlich isotherms for crystal violet adsorption by PrAC, BAC, and CAC at 30°C, 40°C, 50°C, and 60°C and pH 5.0.

Table 8 indicate endothermic adsorption with positive values of $\Delta H°$ (18.432 kJ mol^{-1} for PrAC and 16.490 kJ mol^{-1} for BAC). The positive values of $\Delta S°$ (0.063 kJ mol^{-1}K^{-1} for PrAC and 0.067 kJ mol^{-1}K^{-1} for BAC) suggest that the degree of randomness at the solid-liquid interface increases with adsorption of crystal violet on both PrAC and BAC [51,52]. The negative values of $\Delta G°$ at all temperatures confirm the thermodynamic feasibility and spontaneity of crystal violet sorption onto PrAC and BAC.

3.4. Desorption study

The percentage of desorbed crystal violet decreased from 67.08 to 49.05 for CAC, from 46.32 to 32.86 for PrAC, and from 40.64 to 24.48 for BAC, as pH increased from 2.03 to 8.98 (Fig. 14). The trend in desorption against pH was opposite to that for adsorption (Fig. 10). This indicates that adsorption of the dye was mainly of physical type, and PrAC and BAC can be reused, which may contribute positively to the economy of the treatment process [59].

3.5. Application to treatment of textile wastewater

PrAC and BAC were tested on textile wastewater collected from a local factory in Hat Yai, Songkhla, Thailand. Crystal violet adsorption on PrAC and BAC was found to be 59.75% and 45.45%, respectively, in the textile wastewater. The initial concentration of crystal violet was 300 mg L^{-1}, at pH 5.

3.6. Cost estimates of PrAC and BAC preparation

The cost of preparing PrAC and BAC from the pericarp of rubber fruit and from bagasse strongly affects whether

Table 5
Parameters of Langmuir isotherm from least-squares fits experimental data on crystal violet adsorption by PrAC, BAC, and CAC at various temperatures

Temp. (°C)	PrAC				BAC				CAC			
	q_m			R^2	q_m			R^2	q_m			R^2
	mmol g^{-1}	mg g^{-1}	b (L mmol^{-1})		mmol g^{-1}	mg g^{-1}	b (L mmol^{-1})		mmol g^{-1}	mg g^{-1}	b (L mmol^{-1})	
30	0.89	362.21	15.18	0.99	0.81	330.90	26.37	0.99	1.68	687.79	57.04	0.99
40	0.95	386.69	24.77	0.99	0.83	336.50	31.82	1.00	1.90	776.11	44.55	0.99
50	1.05	429.88	22.93	0.99	0.85	348.33	37.54	0.99	2.06	838.99	51.19	0.99
60	1.06	432.66	43.87	0.99	0.86	351.12	52.58	0.99	2.20	896.70	89.22	0.99

Table 6
Parameters in Freundlich isotherm fits by least squares to experimental data on crystal violet adsorption by PrAC, BAC, and CAC at various temperatures

Temp (°C)	PrAC			BAC			CAC		
	K_F (L g^{-1})	n	R^2	K_F (L g^{-1})	n	R^2	K_F (L g^{-1})	n	R^2
30	1.01	4.02	0.86	1.03	5.44	0.82	1.11	2.71	0.61
40	1.03	5.90	0.87	1.05	5.57	0.80	2.08	7.12	0.78
50	1.06	7.65	0.84	1.07	6.47	0.81	2.31	7.52	0.79
60	1.20	7.78	0.80	1.14	7.89	0.70	2.55	7.80	0.86

Table 7
Observed maximum adsorption capacities of crystal violet compared with prior literature data

S. No.	Adsorbent	q_m (mg g^{-1})	Ref.
1	Jute fiber carbon	27.99	[48]
2	Coniferous Pinus bark powder AC	32.78	[49]
3	Date palm leaves AC	37.58	[50]
4	NaOH-modified rice husk AC	44.87	[18]
5	*Punica granatum* shell AC	50.21	[51]
6	Male flowers of coconut tree AC	60.42	[20]
7	Rice husk AC	61.58	[26]
8	Tomato paste waste AC	68.97	[53]
9	Palm kernel fiber AC	78.90	[54]
10	Skin almond waste AC	85.47	[55]
11	Korean cabbage waste AC	195.6	[56]
12	Peanut shells AC	220.7	[57]
13	Water hyacinth plants AC	322.58	[58]
14	Pericarp of rubber fruit AC (PrAC)	432.66	This study
	Bagasse AC (BAC)	351.12	

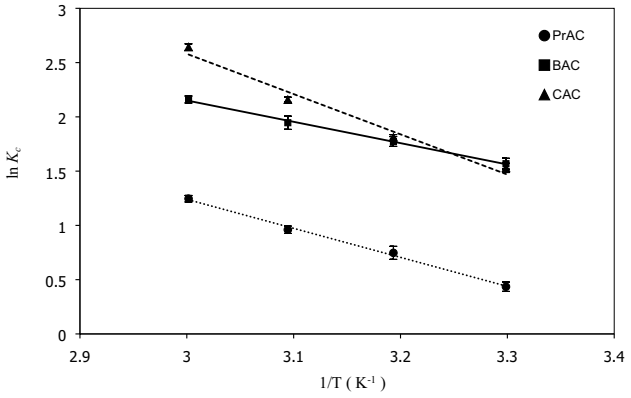

Fig. 13. Van't Hoff plots for adsorption of crystal violet (300 mg L^{-1}) by PrAC, BAC, and CAC at 30°C, 40°C, 50°C, and 60°C, and pH 5.0.

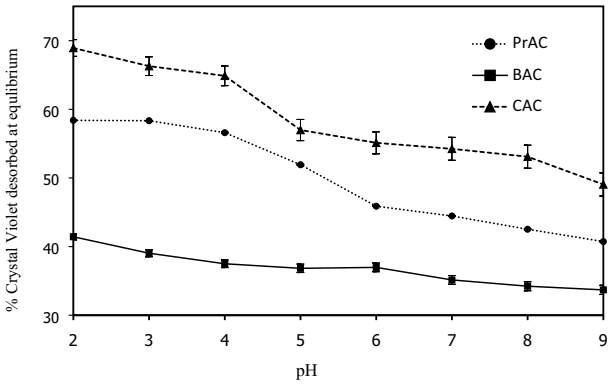

Fig. 14. Desorption of crystal violet on PrAC, BAC, and CAC in pH range 2–9 at 30°C, with 300 mg L^{-1} dye concentration.

either can be used in the removal of crystal violet from aqueous solutions in the industrial scale. Therefore, the cost of adsorbent preparation is of great importance. No cost is placed on the precursor materials here, as pericarp of rubber fruit and bagasse are agricultural wastes. The cost estimates of preparing 1 kg PrAC or BAC are in THB in Table 9.

The net cost equals CRM + CSR + CCD + CCS + CAS = 7 4.59 Baht/adsorbent. Cost estimates of PrAC and BAC production suggest that adsorbent preparation from agricultural wastes is cost-effective, compared to other activated

Table 8
Thermodynamic parameters estimated from van't Hoff equation for crystal violet sorption by PrAC, BAC, and CAC at 30°C, 40°C, 50°C, and 60°C, from initial 300 mg L^{-1} and pH 5.0

Temp. (°C)	PrAC			BAC			CAC		
	$\Delta H°$ (kJ mol^{-1})	$\Delta S°$ (kJ mol^{-1} K^{-1})	$-\Delta G°$ (kJ mol^{-1})	$\Delta H°$ (kJ mol^{-1})	$\Delta S°$ (kJ mol^{-1} K^{-1})	$-\Delta G°$ (kJ mol^{-1})	$\Delta H°$ (kJ mol^{-1})	$\Delta S°$ (kJ mol^{-1} K^{-1})	$-\Delta G°$ (kJ mol^{-1})
30	22.23	0.077	0.79	16.49	0.067	3.77	30.82	0.114	3.71
40			1.43			4.44			4.85
50			2.06			5.11			5.99
60			2.69			5.77			7.13

Table 9
Cost estimates of adsorbent preparation

Cost	THB	Annotation
Cost of raw material (CRM)	0.0	Pericarp of rubber fruit and bagasse are local agricultural wastes
Cost of size reduction (CSR)	0.0	Size reduction was manual with mortar and pestle
Cost of cleaning and drying raw material (CCD)	CW + CD = 3 + 0 = 3	CW = cost of distilled water = 0.015 THB/mL × 200 mL = 3 THB CD = cost of drying = 0.0 Baht, the drying was in sunlight
Cost of carbonization step (CCS)	CH = 12.06	CH = cost of heating (electricity consumption for 1 kg of char electricity power ÷ 1,000 × hour × times × cost of 1 unit) = 1,200 Watt ¸ 1,000 × 1 × 5 × 2.01 = 12.06 THB
Cost of activation step (CAS)	CA + CH + CC = 23 + 36.18 + 0.35 = 59.53	CA = cost of $ZnCl_2$ usage = units × unit per cost × times = 2 × 2. 3 × 5 = 23 THB CH = cost of heating (electricity consumption for 1 kg of adsorbent electricity power ¸ 1,000 × hour × times × cost of 1 u nit) = 1,200 Watt ¸ 1,000 × 3 × 5 × 2.01 = 36.18 THB CC = cost of HCl usage = units × unit per cost × times = 0.2 × 0. 35 × 5 = 0.35 THB
Total	74.59	

carbon products derived from plant biomass [60]. Thus, activated carbon developed from the pericarp of rubber fruit or bagasse can be used as cost-effective adsorbents for dye removal from aqueous solution [61].

4. Conclusion

Crystal violet was adsorbed from aqueous solutions using two candidate adsorbents; activated carbon prepared from the pericarp of rubber fruit powder (PrAC) and activated carbon prepared from carbonized bagasse (BAC); both activated with $ZnCl_2$. The experimental data were reasonably well fit with the Langmuir adsorption isotherm. From these isotherm fits the maximum adsorption capacities (q_m) at 30°C, 40°C, 50°C, and 60°C, were 362.21, 386.69, 429.88, and 432.66 mg g^{-1} for PrAC, 330.90, 336.50, 348.33, and 351.12 mg g^{-1} for BAC and 687.79, 776.11, 838.99, and 898.70 mg g^{-1} for CAC, respectively. The points of zero charge of PrAC, BAC, and CAC were at pH 6.5, 4.5, and 3.5, respectively, which indicates the acidic nature of these activated carbons. The fraction adsorbed decreased with initial crystal violet concentration, and values of ΔH_{ads} between 0 and 40 kJ mol^{-1} confirmed the adsorption as endothermic and dominantly of physical type. The efficiency of the adsorption of crystal violet on PrAC and BAC was about 80% to 90%. Therefore, activated carbon developed from the pericarp of rubber fruit or bagasse can be used as a cost-effective adsorbent for dye removal from aqueous solutions.

Acknowledgments

This research was supported by the Department of Science, Faculty of Science and Technology, Prince of Songkla University, Pattani Campus, Thailand, and by the Department of Chemistry, Prince of Songkla University. Moreover, we would like to acknowledge Asst. Dr. Orawan Sirichote and Asst. Dr. Jareerat Ruamcharoen for suggestions. We are thankful to Dr. Seppo Karrila for assistance with the English language.

References

[1] S.D. Gisi, G. Lofrano, M. Grassi, M. Notarnicola, Characteristics and adsorption capacities of low-cost sorbents for wastewater treatment: a review, Sustainable Mater. Technol., 9 (2016) 10–40.
[2] K. Massoud, S. Mojtaba, M. Sahar, Removal of dyes from the environment by adsorption process, Chem. Mater. Eng., 6 (2018) 31–35.
[3] S. Pattabhi, S. Madhavakrishnan, K. Manickavasagam, R. Vasanthakumar, K. Rasappan, R. Mohanraj, Adsorption of crystal violet dye from aqueous solution using *Ricinus communis* pericarp carbon as an adsorbent, E-J. Chem., 6 (2009) 1109–1116.
[4] M. Simonič, Efficiency of ultrafiltration for the pre-treatment of dye-bath effluents, Desalination, 245 (2009) 701–707.
[5] G. Vijayaraghavana, S. Shanthakumara, Effective removal of reactive magenta dye in textile effluent by coagulation using algal alginate, Desal. Water Treat., 121 (2018) 22–27.
[6] M.H. Mohammad, M.C. Christopher, A critical review on recent advancements of the removal of reactive dyes from dye house effluent by ion-exchange adsorbents, Chemosphere, 209 (2018) 201–219.
[7] R.M. Mohameda, I.A. Mkhalida, S.M. Abdel, M.A. Barakat, Zeolite Y from rice husk ash encapsulated with Ag-TiO_2: characterization and applications for photocatalytic degradation catalysts, Desal. Water Treat., 51 (2013) 7562–7569.
[8] S. Wang, Z.H. Zhu, Effect of acidic treatment of activated carbons on dye adsorption, Dyes Pigm., 75 (2007) 306–314.
[9] C.P.J. Isaac, A. Sivakumar, Removal of lead and cadmium ions from water using *Annona squamosa* shell: kinetic and equilibrium studies, Desal. Water Treat., 51 (2013) 7700–7709.
[10] M. Ishaq, S. Sultan, I. Ahmad, H. Ullah, M. Yaseen, A. Amir, Adsorptive desulfurization of model oil using untreated, acid activated and magnetite nanoparticle loaded bentonite as adsorbent, J. Saudi Chem. Soc., 21 (2017) 143–151.

[11] K.S. Tapan, C.B. Nikhil, K. Subarna, G.A. Mahmooda, I. Hideki, F. Yoshinobu, Adsorption of methyl orange onto chitosan from aqueous solution, J. Water Resour. Prot., 2 (2010) 898–906.
[12] C.R.B. Tharcila, C.I. Juliana, P.M. Carina, A.F. Denise, Adsorption of crystal violet dye from aqueous solution onto zeolites from coal fly and bottom ashes, Orbital: Electron. J. Chem., 5 (2013) 179–191.
[13] M. Belhachemi F. Addoun, Adsorption of congo red onto activated carbons having different surface properties: studies of kinetics and adsorption equilibrium, Desal. Water Treat., 37 (2012) 122–129.
[14] F. Hayeeye, M. Sattar, S. Tekasakul, O. Sirichote, Adsorption of rhodamine B on activated carbon obtained from pericarp of rubber fruit in comparison with the commercial activated carbon, Songklanakarin J. Sci. Technol., 36 (2014) 177–187.
[15] B.H. Hameed, F.B.M. Daud, Adsorption studies of basic dye on activated carbon derived from agricultural waste: *Hevea brasiliensis* seed coat, Chem. Eng. J., 139 (2008) 48–55.
[16] K. Saeed, M. Ishaq, S. Sultan, I. Admad, Removal of methyl violet 2-B from aqueous solutions using untreated and magnetite-impregnated almond shell as adsorbents, Desal. Water Treat., 57 (2016) 13484–13493.
[17] A. Bhatnagar, A.K. Jain, Comparative adsorptions study with different industrial wastes as adsorbents for the removal of cationic dyes from water, J. Colloid Interface Sci., 281 (2005) 49–55.
[18] S. Gupta, B.V. Babu, Economic feasibility analysis of low cost adsorbents for the removal of Cr(VI) from wastewater, Int. J. Civ. Eng. Technol., 10 (2019) 2387–2402.
[19] C. Sagnik, C. Shamik, D.S. Papita, Adsorption of crystal violet from aqueous solution onto NaOH-modified rice husk, Carbohydr. Polym., 86 (2011) 1533–1541.
[20] S. Lairini, K.E. Mahtal, Y. Miyah, K. Tanji, S. Guissi, S. Boumchita, F. Zerrouq, The adsorption of crystal violet from aqueous solution by using potato peels (*Solanum tuberosum*): equilibrium and kinetic studies, J. Mater. Environ. Sci., 8 (2013) 3252–3261.
[21] S. Senthilkumaar, P. Kalaamani, C.V. Subburaam, Liquid phase adsorption of crystal violet onto activated carbons derived from male flowers of coconut tree, J. Hazard. Mater., 136 (2006) 800–808.
[22] K.G. Sandip, K.H. Asim, B. Amitava, Air agitated tapered bubble column adsorber for hazardous dye (crystal violet) removal onto activated ($ZnCl_2$) carbon prepared from bamboo leaves, J. Mol. Liq., 240 (2018) 313–321.
[23] B. McEnaney, F. Schuth, K.S.W. Sing, J. Weitkamp, Chapter 4 – Handbook of Porous Solids, 1st ed., Wiley-VCH Verlag GmbH, Weinheim, Germany, 2002.
[24] R. Azargohar, Production of Activated Carbon and its Catalytic Application for Oxidation of Hydrogen Sulphide, A Thesis, Doctor of Philosophy in the Department of Chemical Engineering University of Saskatchewan, Saskatoon, Canada, 2009.
[25] O. Sirichote, W. Innajitara, L. Chuenchom, S. Panumati, K. Chudecha, P. Vankhaew, V. Choolert, Adsorption of phenol from diluted aqueous solutions by activated carbons obtained from bagasse, oil palm shell and pericarp of rubber fruit, Songklanakarin J. Sci. Technol., 30 (2008) 185–189.
[26] M. Kaustubha, N.J. Thammu, B.C. Meikap, M.N. Biswas, Removal of crystal violet from wastewater by activated carbons prepared from rice husk, Ind. Eng. Chem. Res. Eng., 45 (2006) 5165–5171.
[27] Y.F. Jia, B. Xiao, K.M. Thomas, Adsorption of metal ions on nitrogen surface functional groups in activated carbons, Langmuir, 18 (2002) 470–478.
[28] F. Hayeeye, M. Sattar, W. Chinpa, O. Sirichote, Kinetics and thermodynamics of Rhodamine B adsorption by gelatin/activated carbon composite beads, Colloids Surf., A, 513 (2017) 259–266.
[29] S. Lagergren, Zur theorie der sogenannten adsorption geloster stoffe, Kungliga Svenska Vetenskapsakademiens, Handlingar, 24 (1898) 1–39.
[30] Y.S. Ho, G. McKay, Pseudo-second-order model for sorption processes, Process Biochem., 34 (1999) 451–465.
[31] F.C. Wu, R.L. Tseng, R.S. Juang, Initial behavior of intraparticle diffusion model used in the description of adsorption kinetics, Chem. Eng. J., 153 (2009) 1–8.
[32] W. Weber, J. Morris, Kinetics of adsorption on carbon from solution, J. Sanit. Eng. Div., 89 (1963) 31–60.
[33] F.-C. Wu, R.-L. Tseng, R.-S. Juang, Initial behavior of intra-particle diffusion model used in the description of adsorption kinetics, Chem. Eng. J., 153 (2009) 1–8.
[34] I. Langmuir, Adsorption of gases on plane surfaces of glass, mica and platinum, J. Am. Chem. Soc., 40 (1918) 1361.
[35] H. Freundlich, Uber die adsorption in losungen (adsorption in solution), Z. Phys. Chem., 57 (1906) 384–470.
[36] V.J.P. Poots, G. McKay, J.J. Healy, Removal of basic dye from effluent using wood as an adsorbent, J. Water Pollut. Control Fed., 50 (1978) 926–935.
[37] M. Sattar, F. Hayeeye, W. Chinpa, O. Sirichote, Preparation and characterization of poly (lactic acid)/activated carbon composite bead via phase inversion method and its use as adsorbent for Rhodamine B in aqueous solution, J. Environ. Chem. Eng., 5 (2017) 3780–3791.
[38] J.P. Barford, G. McKay, Reactive Black dye adsorption/desorption onto different adsorbents: effect of salt, surface chemistry, pore size and surface area, J. Colloid Interface Sci., 337 (2009) 32–38.
[39] S. Brunauer, J. Skalny, E.E. Bodor, Adsorption on nonporous solids, J. Colloid Interface Sci., 30 (1969) 546–552.
[40] E.P. Barrett, L.G. Joyner, P.P. Halenda, Pore size distribution for porous materials, J. Am. Chem. Soc., 73 (1951) 373–380.
[41] Z. Hu, E.F. Vansant, A new composite adsorbent produced by chemical activation of elutrilithe with zinc chloride, J. Colloid Interface Sci., 176 (1995) 422–431.
[42] V.J. Strelko, D.J. Malik, Characterization and metal sorption properties of oxidized active carbon, J. Colloid Interface Sci., 250 (2002) 213–220.
[43] B. Stuart, Infrared Spectroscopy: Fundamentals and Applications, John Wiley & Sons Ltd., University of Technology, Sydney, Australia, 2004.
[44] A.A. Jamal, M.O. Sulyman, K.Y. Elazaby, M.A. Salah, Adsorption of Pb(II) and Cu(II) from aqueous solution onto activated carbon prepared from dates stones, Int. J. Environ. Sci. Dev., 4 (2013) 191–195.
[45] A. Thakur, H. Kaur, Response surface optimization of Rhodamine B dye removal using paper industry waste as adsorbent, Int. J. Ind. Chem., 8 (2017) 175–186.
[46] A. Rais, K. Rajeev, Adsorption of amaranth dye onto alumina reinforced poly-styrene, CLEAN–Soil Air Water, 39 (2010) 74–82.
[47] I.A. Umar, G. Abdulraheem, S. Bala, S. Muhammad, M. Abdullahi, Kinetics, equilibrium and thermodynamics studies of C.I. Reactive Blue 19 dye adsorption on coconut shell based activated carbon, Int. Biodeterior. Biodegrad., 102 (2015) 265–273.
[48] K. Porkodi, K.K. Vasanth, Equilibrium, kinetics and mechanism modeling andsimulation of basic and acid dyes sorption onto jute fiber carbon: eosin yellow, malachite green and crystal violet single component systems, J. Hazard. Mater., 143 (2007) 311–327.
[49] R. Ahmad, Studies on adsorption of crystal violet dye from aqueous solution onto coniferous pinus bark powder (CPBP), J. Hazard. Mater., 171 (2009) 767–773.
[50] A. Ghazalia, M. Shiranib, A. Semnania, V. Zare-Shahabadic, M. Nekoeinia, Optimization of crystal violet adsorption onto date palm leaves as a potent biosorbent from aqueous solutions using response surface methodology and ant colony, J. Environ. Chem. Eng., 6 (2018) 3942–3950.
[51] M.B. Silveira, F.A. Pavan, N.F. Gelos, E.C. Lima, S.L. Dias, *Punica granatum* shell preparation, characterization, and use for crystal violet removal from aqueous solution, Clean–Soil Air Water, 42 (2014) 939–946.
[52] A.A. Alqadami, M. Naushad, M.A. Abdalla, M.R. Khan, Z.A. Alothman, Adsorptive removal of toxic dye using Fe_3O_4-TSC nanocomposite: equilibrium, kinetic, thermodynamic studies, J. Chem. Eng. Data, 61 (2016) 3806–3813.
[53] H. Güzel, F. Sayğılı, G.A. Sayğılı, F. Koyuncu, Decolorisation of aqueous crystal violetsolution by a new nanoporous carbon:

equilibrium and kinetic approach, J. Ind. Eng. Chem., 20 (2014) 3375–3386.
[54] G.O. El-Sayed, Removal of methylene blue and crystal violet from aqueous solutions by palm kernel fiber, Desalination, 272 (2011) 225–232.
[55] F. Atmani, A. Bensmaili, N.Y. Mezenner, Synthetic textile effluent removal by skin almonds waste, J. Environ. Sci. Technol., 2 (2009) 153–169.
[56] D.D. Sewu, P. Boakye, S.H. Woo, Highly efficient adsorption of cationic dye by biochar produced with Korean cabbage waste, Bioresour. Technol., 224 (2017) 206–213.
[57] J.X. Zhang, L.L. Ou, Kinetic, isotherm and thermodynamic studies of the adsorption of crystal violet by activated carbon from peanut shells, Water Sci. Technol., 67 (2013) 737–744.
[58] K.M. Rajeswari, T. Revanth, A. Anirudh, B. Prasad, Removal of crystal violet dye from aqueous solution using water hyacinth: equilibrium, kinetics and thermodynamics study, Resour.-Effic. Technol., 3 (2017) 71–77.
[59] D. Ehsan, V. Arya, N. Ali, K. Masoud, N. Mu, B. Amit, Desorption of Methylene blue dye from brown macroalga: effects of operating parameters, isotherm study and kinetic modeling, J. Cleaner Prod., 152 (2017) 443–453.
[60] U. Maheshwari, S. Gupta, Kinetic and equilibrium studies of Cr(VI) removal from aqueous solutions using activated neem bark, Res. J. Chem. Environ., 15 (2011) 939–943.
[61] S. Banerjee, S. Mukherjee, A. LaminKa-ot, S.R. Joshi, T. Mandal, G. Halder, Biosorptive uptake of Fe^{2+}, Cu^{2+} and As^{5+} by activated biochar derived from *Colocasia esculenta*: isotherm, kinetics, thermodynamics, and cost estimation, J. Adv. Res., 7 (2016) 597–610.